JACS ARTICLES

Published on Web 10/01/2009

Coordination-Mode Control of Bound Nitrile Radical Complex Reactivity: Intercepting End-on Nitrile−Mo(III) Radicals at Low Temperature

Meaghan E. Germain,[†] Manuel Temprado,[‡,§] Annie Castonguay,[†] Olga P. Kryatova,[†] Elena V. Rybak-Akimova,[*,†] John J. Curley,[‡] Arjun Mendiratta,[‡] Yi-Chou Tsai,[‡] Christopher C. Cummins,[*,‡] Rajeev Prabhakar,[*,§] James E. McDonough,[§] and Carl D. Hoff[*,§]

Department of Chemistry, Tufts University, 62 Talbot Avenue, Medford, Massachusetts 02155, Department of Chemistry, Massachusetts Institute of Technology, 77 Massachusetts Avenue, Cambridge, Massachusetts 02139, and Department of Chemistry, University of Miami, 1301 Memorial Drive, Coral Gables, Florida 33146

Received July 20, 2009; E-mail: c.hoff@miami.edu

Abstract: Variable temperature equilibrium studies were used to derive thermodynamic data for formation of η^1 nitrile complexes with Mo(N[^{t}Bu]Ar)$_3$, **1**. (1-AdamantylCN = AdCN: $\Delta H^o = -6 \pm 2$ kcal mol^{-1}, $\Delta S^o = -20 \pm 7$ cal mol^{-1} K^{-1}. C_6H_5CN = PhCN: $\Delta H^o = -14.5 \pm 1.5$ kcal mol^{-1}, $\Delta S^o = -40 \pm 5$ cal mol^{-1} K^{-1}. 2,4,6-$(H_3C)_3C_6H_2CN$ = MesCN: $\Delta H^o = -15.4 \pm 1.5$ kcal mol^{-1}, $\Delta S^o = -52 \pm 5$ cal mol^{-1} K^{-1}.) Solution calorimetric studies show that the enthalpy of formation of **1**-[η^2-NCNMe$_2$] is more exothermic ($\Delta H^o = -22.0 \pm 1.0$ kcal mol^{-1}). Rate and activation parameters for η^1 binding of nitriles were measured by stopped flow kinetic studies (AdCN: $\Delta H_{on}^{\ddagger} = 5 \pm 1$ kcal mol^{-1}, $\Delta S_{on}^{\ddagger} = -28 \pm 5$ cal mol^{-1} K^{-1}; PhCN: $\Delta H_{on}^{\ddagger} = 5.2 \pm 0.2$ kcal mol^{-1}, $\Delta S_{on}^{\ddagger} = -24 \pm 1$ cal mol^{-1} K^{-1}; MesCN: $\Delta H_{on}^{\ddagger} = 5.0 \pm 0.3$ kcal mol^{-1}, $\Delta S_{on}^{\ddagger} = -26 \pm 1$ cal mol^{-1} K^{-1}). Binding of Me$_2$NCN was observed to proceed by reversible formation of an intermediate complex **1**-[η^1-NCNMe$_2$] which subsequently forms **1**-[η^2-NCNMe$_2$]: $\Delta H^{\ddagger}_{k1} = 6.4 \pm 0.4$ kcal mol^{-1}, $\Delta S^{\ddagger}_{k1} = -18 \pm 2$ cal mol^{-1} K^{-1}, and $\Delta H^{\ddagger}_{k2} = 11.1 \pm 0.2$ kcal mol^{-1}, $\Delta S^{\ddagger}_{k2} = -7.5 \pm 0.8$ cal mol^{-1} K^{-1}. The oxidative addition of PhSSPh to **1**-[η^1-NCPh] is a rapid second-order process with activation parameters: $\Delta H^{\ddagger} = 6.7 \pm 0.6$ kcal mol^{-1}, $\Delta S^{\ddagger} = -27 \pm 4$ cal mol^{-1} K^{-1}. The oxidative addition of PhSSPh to **1**-[η^2-NCNMe$_2$] also followed a second-order rate law but was much slower: $\Delta H^{\ddagger} = 12.2 \pm 1.5$ kcal mol^{-1} and $\Delta S^{\ddagger} = -25.4 \pm 5.0$ cal mol^{-1} K^{-1}. The crystal structure of **1**-[η^1-NC(SPh)NMe$_2$] is reported. Trapping of *in situ* generated **1**-[η^1-NCNMe$_2$] by PhSSPh was successful at low temperatures (−80 to −40 °C) as studied by stopped flow methods. If **1**-[η^1-NCNMe$_2$] is not intercepted before isomerization to **1**-[η^2-NCNMe$_2$] no oxidative addition occurs at low temperatures. The structures of key intermediates have been studied by density functional theory, confirming partial radical character of the carbon atom in η^1-bound nitriles. A complete reaction profile for reversible ligand binding, η^1 to η^2 isomerization, and oxidative addition of PhSSPh has been assembled and gives a clear picture of ligand reactivity as a function of hapticity in this system.

Introduction

Coordination of a diatomic molecule to a single metal center can be identified with two limiting modes: end-on (η^1) or side-on (η^2), and the same is true for the coordination of certain organic functional groups. In an early study of the coordination chemistry of N_2, Taube showed via isotopic labeling studies that the end-on coordinated N_2 ligand in $[(\eta^1\text{-}N_2)Ru(NH_3)_5]^{2+}$ is able to exchange its terminal with its bound nitrogen, and proposed that this process takes place via an unobserved side-on intermediate, that is, $[(\eta^2\text{-}N_2)Ru(NH_3)_5]^{2+}$.[1] Characterization using X-ray diffraction studies of metastable side-bound N_2 and NO ligands in mononuclear complexes has since been accomplished.[2] Particularly for O_2 as a ligand, it is recognized that both the coordination mode (e.g., η^1 versus η^2) and the spin state (e.g., singlet versus triplet) may vary, giving rise to four possibilities, each of which may be distinguished in terms of the degree of metal to ligand charge transfer, as well as in terms of characteristic ligand stretching frequency.[3] Shan and Que have detected a diiron(II,III) end-on bound superoxide which rearranges to a diiron(III)-hydroperoxide.[4] Shaik et al. have investigated computationally the possibility of a single oxidant with two spin states masquerading as two different oxidants in the Cytochrome P-450 enzyme.[5]

In studies of O_2 binding to biological copper sites, both CO and MeCN have been used as models considered to be "redox-

[†] Tufts University.
[‡] Massachusetts Institute of Technology.
[§] University of Miami.

(1) Armor, J. N.; Taube, H. *J. Am. Chem. Soc.* **1970**, *92*, 2560.
(2) Coppens, P.; Novozhilova, I.; Kovalevsky, A. *Chem. Rev.* **2002**, *102*, 861.
(3) de la Lande, A.; Gérard, H.; Moliner, V.; Izzet, G.; Reinaud, O.; Parisel, O. *J. Biol. Inorg. Chem.* **2006**, *11*, 593.
(4) Shan, X. P.; Que, L. *Proc. Natl. Acad. Sci. U.S.A.* **2005**, *102*, 5340.

10.1021/ja905849a CCC: $40.75

innocent".[3] In the particular case of MeCN, while η^1 binding is more common by far, description of an η^2 binding mode was documented by Wilkinson et al. in the classic organometallic complex $Cp_2Mo(NCMe)$.[6] Metal-activated organonitrile chemistry has received increasing study due to a myriad of catalytic and stoichiometric reactions that have been discovered recently in this area.[7] Templeton has recently reported preparation[8] and subsequent reduction[9] of η^2 nitrile complexes of W(II) monocarbonyl bis(acetylacetonate). Parkin has reported the surprisingly facile alkylation of $(Cp^{tBu})_2Mo(\eta^2\text{-NCMe})$.[10] These and other results have been taken to indicate possible increased reactivity of nitriles in the η^2 binding mode.[11] The binding properties of **:**N≡N**:** are probably best approximated by **:**N≡C−R and thus the bond to nitriles provides a starting point to understanding the bond to dinitrogen with the important difference that variation of the R group in R-C≡N**:** can provide insight into the nature of the $L_nM-N\equiv C-R$ bond. It should be noted that some bonding motifs, such as "side-on−end-on",[12] that are available to N_2 are probably not available to R−C≡N**:**, however for interrogating the nature of the $M-N_2$ bond the Mo−N≡C−R analogy provides a tunable probe.

The nature of the $L_nM-N\equiv C-R$ bond is expected to depend strongly on the nature of the metal complex and its spin state, but changes in the R group of the nitrile can be equally important in determining reactivity. Kukushkin and co-workers[13] have recently shown that changing from a conventional nitrile to a "push-pull nitrile",[14] such as a dialkyl cyanamide, can completely alter the course of nucleophilic addition to Pt(II) complexes. The lone pair of electrons on the dialkyl amino group of $R_2N-C\equiv N$ can become involved in the bonding and reactivity of mixed dinitrogen organocyanamide complexes of Mo(0) as reported also by Pombeiro and co-workers.[15] Notably, the crystal structures of both *trans*-$[Mo(N_2)(NCNEt_2)(dppe)_2]$[15] and $W(P[^iPr]_3)_2(CO)_3(NCNMe_2)$[16] have trigonal planar geometry of the amide group.

A final factor controlling binding and reactivity of nitriles is the hapticity of the nitrile ligand itself. The conclusion discussed earlier that some enhanced reactivity may be expected from η^2 bound nitriles, certainly has precedent in N_2 chemistry where unique activation has been achieved in some systems utilizing more complex binding motifs.[17] Theoretical studies of switching of end-on to side-on coordination in $HCo(L)_3$ complexes predict that hapticity can be controlled by ligand choice and that side on complexes are more activated.[18] However, opportunities to examine reactivity in which both binding modalities can be studied for the same metal complex are rare.

Despite the importance of the metal-nitrile bond there are surprisingly few solution phase studies of bond energetics even for bonding in the terminal mode to diamagnetic complexes. We recently reported thermochemical and computational study of bond energetics of a range of nitriles and other N donor ligands to $Mo(CO)_3(P[^iPr]_3)_2$.[16] While nitriles bound ∼6 kcal mol^{-1} more strongly than N_2, changes in R that caused significant changes in IR frequencies and dramatic changes in color resulted in no real difference in bond strength for the nitriles in eq 1: $\Delta H = 0.0 \pm 0.4$ kcal mol^{-1}, AdCN = 1-adamantyl nitrile, Ar = 4-$NMe_2C_6H_4$; 2,4,6-$Me_3C_6H_2$; 2,6-$F_2C_6H_3$; 4-$CF_3C_6H_4$; F_5C_6.

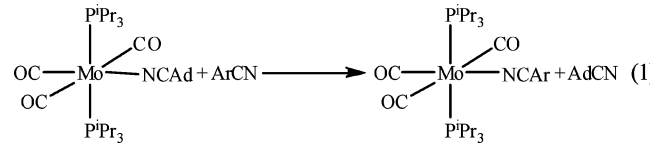

(1)

It seems likely that the thermoneutral character of the Mo-nitrile bond in $Mo(CO)_3(P[^iPr]_3)_2(NCR)$ will not generalize to other complexes. Paramagnetic nitrile complexes in which some spin density is transferred to the nitrile ligand from the metal might be expected to show more ligand dependent energetics.

To the authors' knowledge, the first quantitative data for binding of nitriles to a paramagnetic complex was reported by Kovacs and co-workers[19] for the iron complex $[Fe^{III}(S_2{}^{Me2}N_3(Et,Pr))]^+$ which is a model for nitrile hydratase.[20] In that system, benzonitrile had a less favorable enthalpy of binding ($\Delta H = -4.2 \pm 0.6$ kcal mol^{-1}, $\Delta S = -18 \pm 3$ cal mol^{-1} K^{-1}) than did acetonitrile ($\Delta H = -6.2 \pm 0.2$ kcal mol^{-1}, $\Delta S = -29.4 \pm 0.8$ cal mol^{-1} K^{-1}). Grapperhaus has recently characterized $[LFe-N\equiv C-Me]^+$, L = *N*,*N*′-4,5-bis(2′-methyl-2′-mercaptopropyl)-1-thia-4,7-diazacyclononane, as a new model system for nitrile hydratase which binds acetonitrile with a K_{eq} comparable to that reported for $[Fe^{III}(S_2{}^{Me2}N_3(Et,Pr))]^+$.[21] Such paramagnetic nitrile complexes are frequently observed to be more labile than spin-paired analogues. Kinetic data on rates of binding are scarce, as are structural data on complexes that could be considered to be "bound radicals".[22]

We have shown previously that nitriles may bind both reversibly and in either an η^1 or an η^2 coordination mode to the sterically hindered complex $Mo(N[^tBu]Ar)_3$ **1**, where Ar = 3,5-$C_6H_3Me_2$ (Scheme 1).[23] Furthermore, the same $S = {}^3/_2$ metalloradical complex $Mo(N[^tBu]Ar)_3$ was shown to effect nitrile reductive coupling via slow dimerization of the adduct $(RCN)Mo(N[^tBu]Ar)_3$, with C−C bond formation.[23] In addition, interception of the adduct $(RCN)Mo(N[^tBu]Ar)_3$ using X·

(5) Sharma, P. K.; de Visser, S. P.; Shaik, S. *J. Am. Chem. Soc.* **2003**, *125*, 8698.
(6) Wright, T. C.; Wilkinson, G.; Motevalli, M.; Hursthouse, M. B. *J. Chem. Soc., Dalton Trans.* **1986**, 2017.
(7) Kukushkin, V. Y.; Pombeiro, J. L. *Chem. Rev.* **2002**, *102*, 1771.
(8) Jackson, A. B.; Schauer, C. K.; White, P. S.; Templeton, J. L. *J. Am. Chem. Soc.* **2007**, *129*, 10628.
(9) Jackson, A. B.; Khosla, C.; Gaskins, H. E.; White, P. S.; Templeton, J. L. *Organometallics* **2008**, *27*, 1322.
(10) Shin, J. H.; Savage, W.; Murphy, V. J.; Bonanno, J. B.; Churchill, D. G.; Parkin, G. *J. Chem. Soc., Dalton Trans.* **2001**, 1732.
(11) For additional discussion see ref 7, p 1792.
(12) Fryzuk, M. D. *Acc. Chem. Res.* **2009**, *42*, 127.
(13) Gushchin, P. V.; Kuznetsov, M. L.; Haukka, M.; Wang, M. -J.; Gribanov, A. V.; Kukushkin, V. Y. *Inorg. Chem.* **2009**, *48*, 2583.
(14) Le Questel, J. Y.; Berthelot, M.; Laurence, C. *J. Phys. Org. Chem.* **2000**, *13*, 347. Ziao, N.; Graton, J.; Laurence, C.; Le Questel, J. Y. *Acta Crystallogr., Sect. B* **2001**, *B57*, 850.
(15) Cunha, S. M. P. R. M.; Guedes da Silva, M. F. C.; Pombeiro, A. J. L. *Inorg. Chem.* **2003**, *42*, 2157.
(16) Achord, P.; Fujita, E.; Muckerman, J. T.; Scott, B.; Fortman, G. C.; Temprado, M.; Xiaochen, C.; Captain, B.; Isrow, D.; Weir, J. J.; McDonough, J. E.; Hoff, C. D. *Inorg. Chem.* **2009**, *48*, 7891.
(17) Hidai, M.; Mizobe, Y. *Chem. Rev.* **1995**, *95*, 1115. Fryzuk, M. D.; Johnson, S. A. *Coord. Chem. Rev.* **2000**, *200−202*, 379. MacKay, B. A.; Fryzuk, M. D. *Chem. Rev.* **2004**, *104*, 385.
(18) Huo, C. F.; Zeng, T.; Li, Y. -W.; Beller, M.; Jiao, H. *Organometallics* **2005**, *24*, 6037.
(19) Shearer, J.; Jackson, H. L.; Schweitzer, D.; Rittenberg, D. K.; Leavy, T. M.; Kaminsky, W.; Scarrow, R. C.; Kovacs, J. A. *J. Am. Chem. Soc.* **2002**, *124*, 11417.
(20) Kovacs, J. A. *Chem. Rev.* **2004**, *104*, 825.
(21) O'Toole, M. G.; Bennett, B.; Mashuta, M. S.; Grapperhaus, C. A. *Inorg. Chem.* **2009**, *48*, 2300.
(22) Khusniyarov, M. M.; Weyhermür, T.; Bill, E.; Wieghardt, K. *J. Am. Chem. Soc.* **2009**, *131*, 1208.
(23) Tsai, Y.-C.; Stephens, F. H.; Meyer, K.; Mendiratta, A.; Gheorghiu, M. D.; Cummins, C. C. *Organometallics* **2003**, *22*, 2902.

Scheme 1

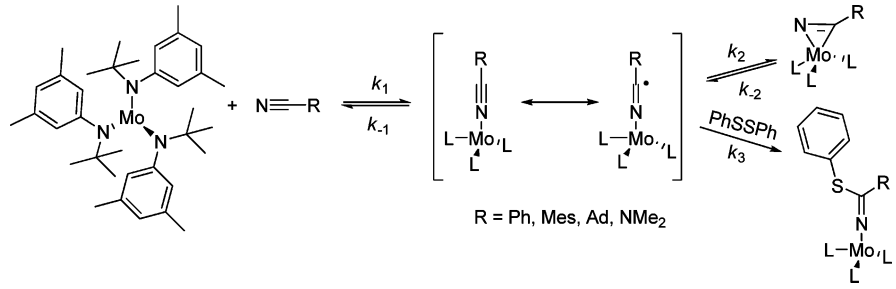

donors such as Ar′EEAr′ (E = S, Se, Te; Ar′ = C_6H_5, C_6F_5) or benzoyl peroxide allowed for generation of C−X bonds in resultant ketimide complexes, R(X)C=N−Mo(N[^{t}Bu]Ar)$_3$.[24] It also allowed for reductive cross-coupling reactions of benzonitrile with pyridine, and with CO_2.[25] Furthermore, when a solution of PhCN-Mo(N[^{t}Bu]Ar)$_3$ is treated with 1 equiv of crystalline HMo(CO)$_3$Cp or 0.5 equiv of $H_2Sn(n\text{-}Bu)_2$ isolation of Ph(H)CN−Mo(N[^{t}Bu]Ar)$_3$ can be achieved.[26]

Though originally formulated as an η^2 complex based on its EPR spectrum,[23] the adduct between benzonitrile and **1** is now known to bind as a terminal η^1 complex.[26,27] In contrast, the crystal structure of the η^2 adduct of **1** and dimethyl cyanamide has been determined[23] and leaves no doubt regarding its hapticity. In the course of forming its η^2 adduct, N≡C−NMe$_2$ would be expected to proceed via an initial η^1 complex which could be either more or less reactive than the final η^2 adduct. This work takes advantage of this unique situation to investigate in detail the binding and reactivity of **1** with nitriles in which different hapticities are accessible and can be kinetically resolved for the same metal complex in reactions with radical coupling partners, such as diphenyldisulfide (Scheme 1).

Results

Spectroscopic and Equilibrium Studies of η^1 Binding of Nitriles to 1. Addition of excess R-C≡N (R = Ph, C_6H_5; Mes, 3,5-$(H_3C)_2C_6H_3$; Ad, 1-adamantyl) to toluene solutions of **1** leads to rapid establishment of the equilibrium shown in eq 2.

$$\text{Mo(N[}t\text{-Bu]Ar)}_3 + \text{RCN} \underset{k_{-1}}{\overset{k_1}{\rightleftharpoons}} (\eta^1\text{-RCN})\text{Mo(N[}t\text{-Bu]Ar)}_3 \qquad (2)$$

The equilibrium is characterized by a dramatic change in color to deep purple and also produces a strong and broad infrared absorption band in the range 2100−2000 cm^{-1} characteristic of the η^1 bound complexes. The $\nu_{C\equiv N}$ band is shifted to significantly lower wavenumbers (by 150−200 cm^{-1}) upon coordination to **1**. Increasing the bulky nature of the nitrile shifts the equilibrium to the reagents and thus, more RCN and lower temperatures are required to achieve complete conversion to **1**-[η^1-NCR]. Because of the extremely weak binding in the case of AdCN, concentrated solutions of nitrile ≈ 0.6 M were needed to observe binding by **1** ≈ 0.02 M in toluene in the temperature range 18 to −65 °C. Quantitative determination of K_{eq} for RCN binding to **1** was made by Fourier transform-infrared (FT-IR) spectroscopy. Spectroscopic data and van't Hoff plots for binding of these nitriles (Figures S1 and S2 in Supporting Information) allow derivation of the thermodynamic and spectroscopic parameters collected in Table 1.

Table 1. Thermodynamic (ΔH^o in kcal mol^{-1} and ΔS^o in cal mol^{-1} K^{-1}) and Spectroscopic Data (cm^{-1}) for Binding of Nitriles to **1** in Toluene Solution

	1-[η^1-NCPh]	**1**-[η^1-NCMes]	**1**-[η^1-NCAd]
ΔH^o	−14.5 ± 1.5	−15.4 ± 1.5	−6 ± 2
ΔS^o	−40 ± 5	−52 ± 5	−20 ± 7
$\nu_{C\equiv N\ free}$	2231	2220	2234
$\nu_{C\equiv N\eta 1\ bound}$	2035	2023	2079
$\Delta\nu_{C\equiv N(\eta 1)}$	−196	−197	−155

Thermodynamics of Dimethylcyanamide Binding to 1. In contrast to RCN (R = Ph, Mes, Ad) it was observed previously[23] that binding of dimethylcyanamide was quantitative at room temperature and this allowed calorimetric determination of its enthalpy of binding by two separate methods. The first was direct measurement based on reaction 3.

$$\text{Mo(N[}t\text{-Bu]Ar)}_3 + \text{Me}_2\text{NCN} \xrightarrow{\Delta H = -21.6 \pm 1.4\ \text{kcal mol}^{-1}} (\eta^2\text{-Me}_2\text{NCN})\text{Mo(N[}t\text{-Bu]Ar)}_3 \qquad (3)$$

The enthalpy of reaction 3 was measured using solid **1** as limiting reagent and then corrected for the enthalpy of solution of the complex to give the final derived value with all species in toluene solution. Because this depended on the purity of the highly air sensitive **1**, a second approach was sought. Previously the enthalpy of binding of adamantyl isonitrile was reported by us (reaction 4).[28]

$$\text{Mo(N[}t\text{-Bu]Ar)}_3 + \text{AdNC} \xrightarrow{\Delta H = -29.1 \pm 0.4\ \text{kcal mol}^{-1}} (\eta^1\text{-AdNC})\text{Mo(N[}t\text{-Bu]Ar)}_3 \qquad (4)$$

Investigation of displacement of Me$_2$NCN by AdNC was performed as shown in eq 5.

Subtraction of reaction 4 from reaction 5 yields reaction 3, giving a value of $\Delta H^o = -22.3 \pm 1.0$ kcal mol^{-1} for the enthalpy of reaction 3. This is in good agreement with that measured directly, and we adopt the average of these two measurements, $\Delta H^o = -22.0 \pm 1.0$ kcal mol^{-1}, for the enthalpy of binding of Me$_2$NCN to **1** forming the η^2-complex.

(24) Mendiratta, A.; Cummins, C. C.; Kryatova, O. P.; Rybak-Akimova, E. V.; McDonough, J. E.; Hoff, C. D. *Inorg. Chem.* **2003**, *42*, 8621.
(25) Mendiratta, A.; Cummins, C. C. *Inorg. Chem.* **2005**, *44*, 7319.
(26) Temprado, M.; McDonough, J. E.; Mendiratta, A.; Tsai, Y.-C.; Fortman, G. C.; Cummins, C. C.; Rybak-Akimova, E. V.; Hoff, C. D. *Inorg. Chem.* **2008**, *47*, 9380.
(27) Mendiratta, A.; Cummins, C. C.; Kryatova, O. P.; Rybak-Akimova, E. V.; McDonough, J. E.; Hoff, C. D. *J. Am. Chem. Soc.* **2006**, *128*, 4881.
(28) Stephens, F. H.; Figueroa, J. S.; Cummins, C. C.; Kryatova, O. P.; Kryatov, S. V.; Rybak-Akimova, E. V.; McDonough, J. E.; Hoff, C. D. *Organometallics* **2004**, *23*, 3126.

$$(\eta^2\text{-Me}_2\text{NCN})\text{Mo(N[}t\text{-Bu]Ar)}_3 + \text{AdNC} \xrightarrow{\Delta H = -6.8 \pm 0.6 \text{ kcal mol}^{-1}} (\eta^1\text{-AdNC})\text{Mo(N[}t\text{-Bu]Ar)}_3 + \text{Me}_2\text{NCN} \quad (5)$$

Kinetics of PhCN, MesCN, and AdCN Binding to 1. The rates of binding of nitriles (PhCN, MesCN, AdCN) to **1** were determined by stopped-flow kinetics by following the build-up of the characteristic intense absorption bands of the nitrile complexes in the visible region (Figure 1 and Figure S3). In contrast to the more complex kinetic picture found for binding of Me_2NCN (discussed in a later section), the kinetic traces for binding could be fit to single exponential functions with $k_{obs} = k_1[RCN] + k_{-1}$. Resolution of k_{obs} into its k_1 and k_{-1} components was carried out graphically as shown in Figure 2 from plots of k_{obs} versus [RCN] which have slopes of k_1 and intercepts of k_{-1}. Data for the slope (k_1) is generally known to higher accuracy than data for the intercept (k_{-1}) as is typical in this type of analysis.

Collected values derived from data in Figure 2, including kinetic determination of K_{eq} as a function of temperature by this method are reported in Table S1. Activation parameters were derived using Eyring plots as shown in Figure S4. Kinetic data for these nitriles are summarized in Table 2.

Data in Table 2 can be used to calculate the enthalpies of nitrile binding: PhCN (−8 kcal mol^{-1}); MesCN (−4 kcal mol^{-1}); AdCN (−6 kcal mol^{-1}) and entropies of nitrile binding PhCN (−25 cal mol^{-1} K^{-1}); MesCN (−10 cal mol^{-1} K^{-1}); and AdCN (−24 cal mol^{-1} K^{-1}). These data, except for AdCN, are in only poor agreement with FT-IR data reported earlier in Table 1 which are believed to be more accurate. The equilibrium constant for binding of PhCN was independently determined by UV−vis spectroscopy at room temperature by titration as shown in Figure S5. The derived value of $K_{eq} = 156$ M^{-1} at 20 °C is in reasonable agreement with that determined by FT-IR studies of 116 M^{-1}. The value derived by the purely kinetic method $K_{eq} = k_1/k_{-1} = 45$ M^{-1} is reasonable at this temperature but diverges as the temperature decreases due to differences in resolution of ΔH and ΔS. It should also be considered when comparing data obtained by different techniques that the FT-IR data was obtained generally in more concentrated solution and at higher temperatures than the stopped flow data.

Kinetics of Dimethylcyanamide Binding to 1. Stopped-flow kinetic studies of the reaction between **1** and Me_2NCN gave the first indication of the formation of a detectable η^1-adduct formed on route to the final η^2-complex in keeping with the general kinetic scheme shown in reactions 6 and 7:

$$\text{Mo(N[}t\text{-Bu]Ar)}_3 + \text{Me}_2\text{NCN} \underset{k_{-1}}{\overset{k_1}{\rightleftharpoons}} (\eta^1\text{-Me}_2\text{NCN})\text{Mo(N[}t\text{-Bu]Ar)}_3 \quad (6)$$

$$(\eta^1\text{-Me}_2\text{NCN})\text{Mo(N[}t\text{-Bu]Ar)}_3 \underset{k_{-2}}{\overset{k_2}{\rightleftharpoons}} (\eta^2\text{-Me}_2\text{NCN})\text{Mo(N[}t\text{-Bu]Ar)}_3 \quad (7)$$

The intermediate proposed to be **1**-[η^1-NCNMe$_2$] with an intense absorption at $\lambda = 456$ nm ($\varepsilon = 5670$ M^{-1} cm^{-1}) rapidly accumulates, and then undergoes a transformation into the final product, with electronic transitions that are in agreement with the previously characterized η^2-coordinated complex ($\lambda = 650$ nm, $\varepsilon = 1000$ M^{-1} cm^{-1}). The absorbance spectrum of the η^1-coordinated complex was generated by computer subtraction as shown in Figure S6.

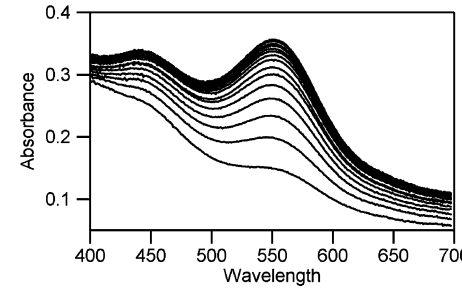

Figure 1. PhCN binding to **1** over $t = 1$ s. [Mo(N[^{t}Bu]Ar)$_3$] = 0.15 mM, [PhCN] = 0.75 mM, −20 °C. Concentrations are listed after mixing in the stopped-flow cell. For the absorption band of **1**-[η^1-NCPh], $\lambda = 560$ nm, $\epsilon = 3000$ M^{-1} cm^{-1}.

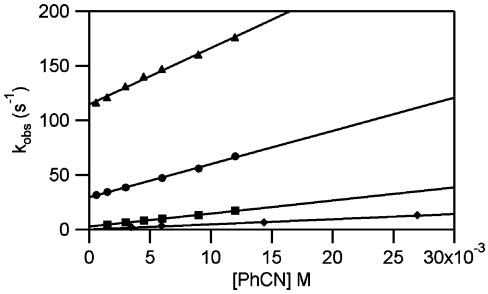

Figure 2. Second-order rate plot for binding of PhCN to **1**, at $T = -40$ (♦),−20 (■), 5 (●), and 20 °C (▲) with [Mo(N[^{t}Bu]Ar)$_3$] = 0.15 mM.

Table 2. Activation Parameters Derived from Eyring Plots, Rate Constants, and Equilibrium Constants for RCN Adducts

	PhCN	MesCN	AdCN
$\Delta H_{on}^{\ddagger}$ (kcal mol^{-1})	5.2 ± 0.2	5.0 ± 0.3	5 ± 1
$\Delta S_{on}^{\ddagger}$ (cal mol^{-1} K^{-1})	−24 ± 1	−26 ± 1	−28 ± 5
$\Delta H_{off}^{\ddagger}$ (kcal mol^{-1})	14 ± 1	9 ± 1	11 ± 1
$\Delta S_{off}^{\ddagger}$ (cal mol^{-1} K^{-1})	0	−18 ± 5	−4 ± 3
k_{on} (M^{-1} s^{-1})[a]	468 ± 22	193 ± 14	97[b]
k_{off} (s^{-1})[a]	0.15 ± 0.3	1.6 ± 0.1	55[b]
K_{eq} (M^{-1})[a]	3120 ± 22	121 ± 14	2[b]

[a] Values reported for $T = -40$ °C. [b] Values extrapolated for $T = -40$ °C.

Stopped-flow kinetic studies of the accumulation and decay of the intermediate species were possible for temperatures varying from −80 to 0 °C. Typical spectroscopic data and a kinetic trace are shown in Figure 3 where the build-up and decay of the intermediate complex at $\lambda = 456$ nm is readily followed.

At 25 °C, the process of intermediate formation becomes too fast and only its decay into the final η^2-complex can be readily observed. Also, the hydrolytic decomposition of complex **1** in the stopped-flow cell became notable above 0 °C, and kinetic data became noisy and poorly reproducible. Therefore, higher-temperature results were excluded from the final analysis. The decay of the absorption band with $\lambda = 456$ nm and the growth of the band with $\lambda = 650$ nm occur on the same time scale. For technical reasons, the kinetics of end-on to side-on conversion of the cyanamide adduct were best followed at 456 nm.[29]

(29) The main reason is that the absorbance was higher at this wavelength, and the higher sensitivity of the detector allowed for dramatically better signal-to-noise ratios on the kinetic traces. Analysis at the 650 nm was found to be in agreement with the analysis at 456 nm^{-1}.

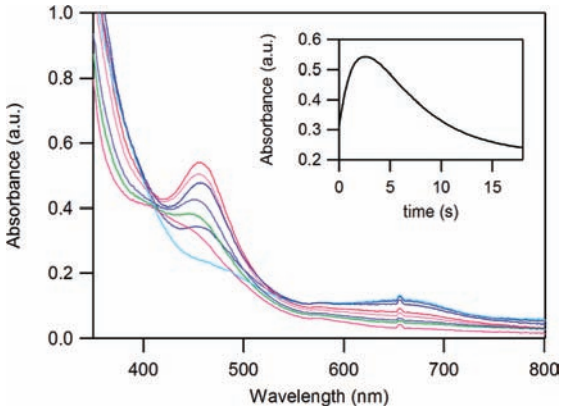

Figure 3. Spectral changes and kinetic trace (at 456 nm) obtained upon mixing at −60 °C toluene solutions of **1** (0.15 mM) and Me_2NCN (1.5 mM). Concentrations are listed after mixing in a stopped-flow cell. Inset: Kinetic trace at 456 nm.

Kinetic measurements were performed under pseudo-first-order conditions (5−300-fold excess of Me_2NCN) over a range of temperatures and fit to the general two term rate law shown in eq 8 which represents a general solution to the mechanism in eqs 6 and 7.

$$\text{rate} = a\mathrm{e}^{-k_{1\text{obs}}t} + b\mathrm{e}^{-k_{2\text{obs}}t} \quad (8)$$

The exponential roots, $k_{1\text{obs}}$ and $k_{2\text{obs}}$ can be a complex function of the three first-order rate constants (k_{-1}, k_2, and k_{-2}) and the pseudo-first-order rate constant $k_1[Me_2NCN]$ in reactions 6 and 7.[30] The change in relative magnitudes of the rate constants as a function of temperature and nitrile concentration, as well as the highly air and moisture sensitive nature of the reactants, made this a challenging system to analyze. Room temperature studies described later showed that ligand displacement and oxidative addition reactions of **1**-[η^2-$NCNMe_2$] occurred on a time scale much slower than that observed in the stopped-flow. From this it can be concluded that $k_{-2} \ll k_1$, k_{-1}, k_2, and so under stopped-flow conditions we assume $k_{-2} \approx 0$.[31]

Fitting of kinetic data to general eq 8 was excellent and showed negligible residual traces. Two limiting temperature regimes became apparent during this work. At low temperature (−80 to ca. −40 °C) the value of k_{-1}, as discussed below, is vanishingly small and no significant contribution to $k_{1\text{obs}}$ from k_{-1} was observed.[32] Thus, the reaction sequence in eqs 6 and 7 simplifies to two consecutive irreversible processes. In that case the exponential roots $k_{1\text{obs}}$ and $k_{2\text{obs}}$ correspond simply to $k_1[Me_2NCN]$ and k_2. At higher temperatures, (−40 to 0 °C) this assumption is no longer valid since the reversible nature of the first step was found to play a role in the kinetic sequence shown in eqs 6 and 7, and more complex analysis was needed. Separation of these two regimes is somewhat arbitrary; however, the general behavior is illustrated in Figure 4 where plots of $k_{1\text{obs}}$ versus nitrile concentration as a function of temperature are displayed.

The increasing value of the intercept with increasing temperature in the main plot and a 0 °C inset of Figure 4 is due to

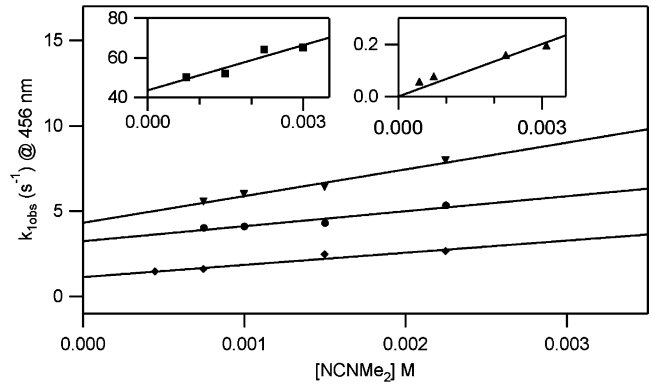

Figure 4. Pseudo-first-order kinetics for 0.15 mM **1** and $[Me_2NCN]$ ranging from 0.75 to 3.1 mM after mixing at −40 (♦), −32 (●), and −28 °C (▼). Inset: 0 (■) and −80 °C (▲).

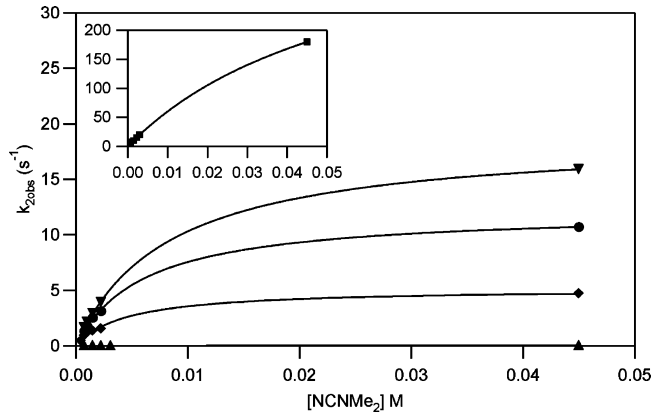

Figure 5. Saturation curves of $k_{2\text{obs}}$ dependence on $[Me_2NCN]$ (measured from decay of 456 nm band) at −80 (▲), −40 (♦), −32 (●), and −28 °C (▼). Inset: 0 °C (■).

the increasing contribution of k_{-1} to $k_{1\text{obs}}$ as was seen earlier for PhCN. As shown in the inset in Figure 4, at low temperature the intercept can be taken as 0 within experimental error.

In addition, the observed rate constant for the second reaction step, $k_{2\text{obs}}$ was found to be independent of Me_2NCN concentration at lower temperatures. However, there is a dependence of $k_{2\text{obs}}$ on nitrile concentration as shown in Figure 5 at temperatures above −40 °C.[33]

Resolution of the data into the separate individual rate constants at higher temperatures (T from −40 to 0 °C) was done using the Specfit program.[34,35] The combined rate data for both low and high temperature regimes are combined in Table 3 and show how the numerical variation of the rate data change as a function of temperature. An important aspect of these data is the increasing significance of k_{-1} relative to k_2 with increasing temperature. The greatest uncertainty in these data are the estimates for k_{-1}, particularly at −40 °C where its value is quite small compared to k_2. Owing to uncertainties in the exact assessment of k_{-1}, derivation of activation parameters as well

(30) Capellos, C.; Bielski, B. H. J. *Kinetic Systems—Mathematical Description of Chemical Kinetics in Solution*; R. E. Krieger: Huntington, NY, 1980.
(31) It is certainly true that $k_{-2} \ll k_2$ since K_{eq} strongly favors the η^2 over η^1 binding mode in this complex.
(32) This division is arbitrary, but examination of data in Table 3 shows that only above −40 °C does k_{-1} become significant relative to the other rate constants.
(33) Despite the fact that $k_{2\text{obs}}$ depends on $[NCNMe_2]$, it was confirmed separately by Specfit analysis that, as expected, k_2 does not.
(34) *SPECFIT Global Analysis System*, version 2.11; Spectrum Software Associates: Singapore.
(35) A number of other analytical methods were attempted, and they were in qualitative agreement with the Specfit but the best overall quantitative treatment of this data was done with this program. The qualitative agreement between these methods indicated a relatively "soft" surface for resolving the rate data, and the low temperature data is believed to be most accurate.

Table 3. Directly Measured (−80 to −50 °C) and Derived (−40 to 0 °C) Rate Constants[a] for Reactions 6 and 7

temperature (°C)	k_1 (M^{-1} s^{-1})	k_{-1} (s^{-1})	k_2 (s^{-1})
−80	52		0.03
−70	55		0.1
−60	145		0.5
−50	361		1.7
−40	708	0.001	4.2
−32	879	0.08	11.4
−28	1563	4	16.1
0	7606	110	179.9

[a] Data for k_1 and k_2 are accurate with errors of less than 10% of the specific value. Derived values for k_{-1} are subject to greater errors and considered as approximate as discussed in the text.

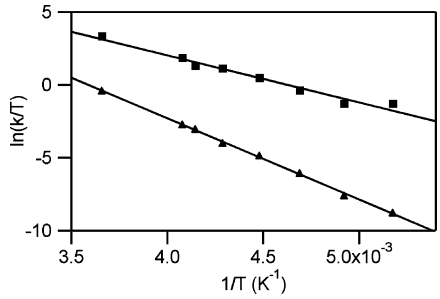

Figure 6. Eyring plot (−80 to 0 °C) for k_1 and k_2 of reactions 6 and 7 from which activation parameters $\Delta H^{\ddagger}_{k1} = 6.4 \pm 0.4$ kcal mol^{-1}, $\Delta S^{\ddagger}_{k1} = -18 \pm 2$ cal mol^{-1} K^{-1}, $\Delta H^{\ddagger}_{k2} = 11.1 \pm 0.2$ kcal mol^{-1}, and $\Delta S^{\ddagger}_{k2} = -7.5 \pm 0.8$ cal mol^{-1} K^{-1} are derived.

as estimates of K_{eq} on a quantitative basis are not warranted. It is clear from the data, however, that k_{-1} begins to play a kinetic role above −40 °C.[36]

In contrast to difficulties in quantitative assignment of k_{-1}, the data for k_1 and k_2 over the entire range of −80 to 0 °C present a consistent picture as summarized in Table 3. The Eyring plot of the combined data shown in Figure 6 gives additional confidence to the Specfit analysis of the high temperature data since there is a seamless fit between the two temperature regimes. From these data the following activation parameters are derived: $\Delta H_1^{\ddagger} = 6.4 \pm 0.4$ kcal mol^{-1}, $\Delta S_1^{\ddagger} = -18 \pm 2$ cal mol^{-1} K^{-1}, $\Delta H_2^{\ddagger} = 11.1 \pm 0.2$ kcal mol^{-1}, and $\Delta S_2^{\ddagger} = -7.5 \pm 0.8$ cal mol^{-1} K^{-1}.

Low-Temperature FT-IR Study of Binding of Me_2NCN to 1. To detect an η^1 intermediate in the binding of Me_2NCN to **1**, detected in stopped-flow UV−vis experiments described above, the FT-IR spectrum of solutions of **1** and excess Me_2NCN were studied in the first 200 s of mixing at −75 ± 5 °C. As shown in Figure S7, a weak band near 1570 cm^{-1} is formed initially and assigned to the intermediate which is proposed to be **1**-[η^1-$NCNMe_2$] based on DFT calculations indicating a weak absorbance in this region as discussed later. As the 1570 cm^{-1} band decreases, bands near 1650 and 1600 cm^{-1} increase and are assigned to **1**-[η^2-$NCNMe_2$]. A plot of ln[A] versus time for these data give an apparent first order rate constant for this interconversion of 0.022 s^{-1} as shown in Figure S8 in agreement to the one determined by stopped-flow methods (Table S1) confirming that the same process is being observed.

Rate of Ligand Displacement from 1-[η^2-$NCNMe_2$] by AdNC Forming 1-[η^1-CNAd]. As stated previously, the enthalpy of the reaction of Me_2NCN displacement from **1**-[η^2-$NCNMe_2$] by AdNC (reaction 5) was determined calorimetrically to indirectly derive the enthalpy of binding of Me_2NCN to **1**. In addition, the rate of reaction 5 was conveniently followed by FT-IR spectroscopy of either decay of free AdNC or build-up of free Me_2NCN as shown in Figure S9. In the presence of excess AdNC excellent first-order kinetic plots were obtained and the reaction was found to be first order in **1** and independent of AdNC concentration provided it was present in modest excess. Activation parameters, $\Delta H^{\ddagger} = 25.6 \pm 0.6$ kcal mol^{-1} and $\Delta S^{\ddagger} = 14.4 \pm 2.1$ cal mol^{-1} K^{-1}, were derived from the Eyring plot shown in Figure S10. These results are in agreement with the enthalpy of nitrile binding of -22.0 ± 1.0 kcal mol^{-1} in **1**-[η^2-$NCNMe_2$] (vide supra) and a mechanism in which complete dissociation of Me_2NCN is the rate determining step followed by rapid trapping by AdNC.

Rate of Oxidative Addition of PhSSPh to 1-[η^1-NCPh]. The rate of reaction 9 was investigated by stopped-flow kinetics using techniques similar to those reported earlier for analogous reactions of PhTeTePh.[24]

$$(\eta^1\text{-PhCN})\text{Mo(N[}t\text{-Bu]Ar)}_3 + \frac{1}{2}\text{PhSSPh} \rightarrow (\eta^1\text{-PhC(SPh)N)Mo(N[}t\text{-Bu]Ar)}_3 \quad (9)$$

Addition of PhSSPh to **1**-[η^1-NCPh] is a relatively rapid process. Reaction of **1** with PhSSPh is slow as shown in Figure S11 and was found to not interfere with the target oxidative addition of PhSSPh to **1**-[η^1-NCPh]. Representative UV−vis data for reaction 9 are shown in Figure S12.

Formation of the ketimide was found to be a clean second-order process (first order in **1**-[η^1-NCPh], and first order in PhSSPh). The concentration dependence from [PhSSPh] at −10 °C under pseudo-first-order conditions gave a linear plot with almost zero (4%) intercept as shown in Figure S13. Collected rate constants in the temperature range −20 to +5 °C were used to derive the activation parameters $\Delta H^{\ddagger} = 6.7 \pm 0.6$ kcal mol^{-1}, $\Delta S^{\ddagger} = -27 \pm 4$ cal mol^{-1} K^{-1} as shown in Figure S14. The enthalpy of activation of this reaction is significantly higher than the value reported earlier for the Te-analogue, **1**-[η^1-NC(TePh)Ph], $\Delta H^{\ddagger} = 3.8$ kcal mol^{-1}, $\Delta S^{\ddagger} = -29$ cal mol^{-1} K^{-1}, in agreement with higher S−S bond enthalpy.[26] Solution calorimetric data for reaction 9 were reported previously with $\Delta H^{o} = -27.1 \pm 0.3$ kcal mol^{-1}.[27]

Synthesis and X-ray Structure of 1-[η^1-NC(SPh)NMe_2]. Green **1**-[η^2-$NCNMe_2$] reacts with PhSSPh as shown in eq 10 in an analogous fashion to **1**-[η^1-NCPh],[27] albeit at an attenuated rate.

$$(\eta^2\text{-Me}_2\text{NCN)Mo(N[}t\text{-Bu]Ar)}_3 + \frac{1}{2}\text{PhSSPh} \rightarrow (\eta^1\text{-Me}_2\text{NC(SPh)N)Mo(N[}t\text{-Bu]Ar)}_3 \quad (10)$$

The solid-state structure of **1**-[η^1-NC(SPh)NMe_2] is shown in Figure 7.

The structure of **1**-[η^1-NC(SPh)NMe_2] is similar to that of **1**-[η^1-NC(SPh)Ph][24] but the former contains a longer Mo−N (1.8325 vs 1.801 Å) and a shorter N═C (1.281 vs 1.322 Å) bond. The same differences were noticed for the calculated geometries of **1**-[η^1-NCPh] and **1**-[η^1-Me_2NCN] as discussed later.

(36) At still higher temperatures, k_{-2} can be expected to contribute to the complex rate law for equations 6 and 7 when all of the rate constants are nontrivial.

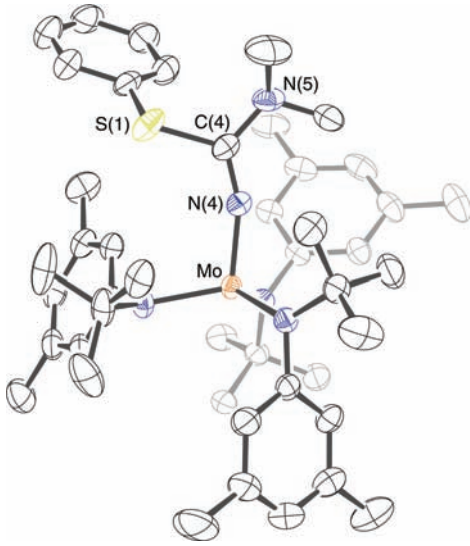

Figure 7. Thermal ellipsoid plot (50% probability) of **1**-[η^1-NC(SPh)NMe_2]. Selected distances (Å) and angles (deg): Mo−N(4), 1.8325(15); N(4)−C(4), 1.281(2); C(4)−S(1), 1.775(2); C(4)−N(5), 1.410(3); Mo−N_{amide}, 1.960 (average); Mo−N(4)−C(4), 161.30(15); N(4)−C(4)−N(5), 124.09(18). Hydrogen atoms have been omitted for clarity.

Rate and Thermochemistry of Oxidative Addition of PhSSPh to 1-[η^2-NCNMe$_2$]. Owing to its slow rate, reaction 10 was investigated using conventional UV−vis techniques. The reaction was run under pseudo-first-order conditions with a large excess of PhSSPh in toluene solution at 15, 30, and 40 °C. Plots of k_{obs} versus [PhSSPh] shown in Figure S15 were found to be linear with near zero intercept. An Eyring plot of these rate data is shown in Figure S16 from which $\Delta H^{\ddagger} = 12.2 \pm 1.5$ kcal mol^{-1} and $\Delta S^{\ddagger} = -25.4 \pm 5.0$ cal mol^{-1} K^{-1} were derived.

The enthalpy of reaction 10 was measured using Calvet calorimetry as $\Delta H = -10.0 \pm 0.5$ kcal mol^{-1}. The considerably less exothermic nature of the oxidative addition of PhSSPh to **1**-[η^2-NCNMe$_2$] compared to the PhCN derivative ($\Delta H^{o} = -27.1 \pm 0.3$ kcal mol^{-1})[27] is due in part to the greater stability of **1**-[η^2-NCNMe$_2$] compared to **1**-[η^1-NCPh] whose bond strengths differ by 22.0 − 14.5 = 7.5 kcal mol^{-1}. However, considerable difference in the stabilities of the ketimide complexes formed must also exist based on the difference of ≈ 17 kcal mol^{-1} in enthalpies of formation.

Low Temperature Stopped-Flow Study of Reaction of 1 and Me$_2$NCN/PhEEPh Mixtures (E = S, Se): In Situ Trapping of 1-[η^1-NCNMe$_2$]. The observed build-up at −80 °C of **1**-[η^1-NCNMe$_2$] and its conversion in about 1 min to **1**-[η^2-NCNMe$_2$] suggested that it might be possible to trap the proposed η^1-intermediate prior to its conversion to the more stable η^2-isomer. Control experiments confirmed, as anticipated from extrapolation to low temperature of the room temperature experiments described in the previous section, that under stopped-flow conditions no detectable reaction occurred between **1**-[η^2-NCNMe$_2$] and PhSSPh over 5 min at −80 °C. In addition, as stated before, the reaction of **1** with PhSSPh is slow and was found to not interfere under the conditions employed with the target trapping reaction between PhSSPh and **1**-[η^1-NCNMe$_2$].

A kinetic trace for the reaction of **1** and a mixture of Me$_2$NCN/PhSSPh at −80 °C over 180 s reaction time is shown in Figure 8. Qualitatively, the spectral features for the overall reaction include the growth of the **1**-[η^1-NCNMe$_2$] intermediate species at $\lambda = 456$ nm, followed by its decay and the formation

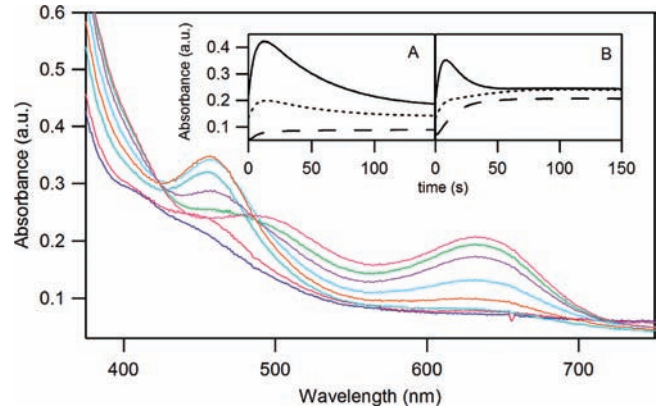

Figure 8. Spectral changes upon addition of PhSSPh to **1**-[η^1-NCNMe$_2$] at −80 °C over $t = 180$ s. Concentrations after mixing: 15, 1.5, 0.15 mM for PhSSPh, Me$_2$NCN, and **1**, respectively; growth and decay at $\lambda = 456$ nm as well as growth at $\lambda = 500$ and 636 nm. Inset: (A) kinetic traces at $\lambda = 456$ nm (solid line), $\lambda = 500$ nm (dotted line), and 636 nm (dashed line) with only Me$_2$NCN added; (B) kinetic traces at $\lambda = 456$ nm (solid line), $\lambda = 500$ nm (dotted line), and 636 nm (dashed line) with both PhSSPh and Me$_2$NCN added.

of two peaks at $\lambda = 500$ and 636 nm, which correspond to the absorbance of the ketimide **1**-[η^1-NC(SPh)NMe_2]. The kinetic traces at these key wavelengths qualitatively describe the differences with and without added PhSSPh. The competing reaction, end-on to side-on isomerization of coordinated dimethylcyanamide, results in the growth of the absorption band with $\lambda = 650$ nm (see above), which partially overlaps with one of the absorption bands of the ketimide at 636 nm, but the latter is narrower and more intense.

Trapping experiments follow the general reaction manifold illustrated in Scheme 1. As expected, the initial rapid growth of the absorbance at 456 nm does not depend on the presence of PhSSPh, and its derived rate constant averaged over all [PhSSPh], $k_{obs} = 0.173$ s^{-1}, corresponds to the previously characterized reaction between **1** and Me$_2$NCN, $k_{obs} = 0.176$ s^{-1}.

A second-order rate plot for the growth of the ketimide species was measured from the growth at $\lambda = 636$ nm and yields a rate constant of $k = 1.9$ M^{-1} s^{-1}, obtained from its slope as shown at the bottom of Figure 9. Because both the η^2 complex and the ketimide product absorb at 636 nm, the intercept of the line at the bottom of Figure 9 cannot be readily used to estimate rate data owing to differences in the extinction coefficient for the two products. The reaction could also be followed by the decay of the absorption at $\lambda = 456$ nm (Figure 9, top). The second-order rate constant generated this way, $k = 1.9 \pm 0.1$ M^{-1} s^{-1} agrees well with the value measured at $\lambda = 636$ nm described above. The intercept on this plot (0.040 ± 0.002 s^{-1}) corresponds to the rate of PhSSPh-independent conversion of **1**-[η^1-NCNMe$_2$] into **1**-[η^2-NCNMe$_2$] (0.04 s^{-1} at −80 °C, Table S1).

Similar trapping experiments were performed under conditions of excess PhSeSePh at −80 °C. This reaction proceeded much more rapidly than with PhSSPh, and the appearance of the **1**-[η^1-NCNMe$_2$] intermediate was hard to detect by eye with high excess of PhSeSePh. The final spectrum of **1**-[η^1-NC(SePh)NMe_2] revealed two peaks that were slightly red-shifted from those due to **1**-[η^1-NC(SPh)NMe_2] at $\lambda = 510$ and 642 nm (Figure S17). As predicted, the observed rates for the decay of the intermediate at $\lambda = 456$ nm as well as the formation of the low energy band at $\lambda = 642$ nm ($k_{obs} = 0.17$ s^{-1} with 7.5

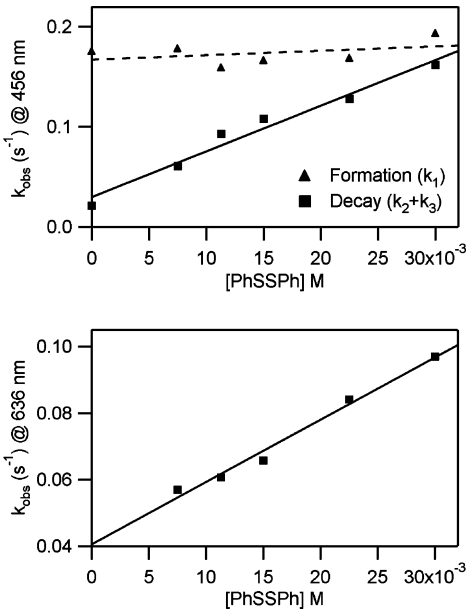

Figure 9. Differences in the formation and decay of the **1**-[η^1-NCNMe$_2$] complex as a function of [PhSSPh], top. Second-order rate plot for the formation of **1**-[η^1-NC(SPh)NMe$_2$], bottom.

mM PhSeSePh) were faster at higher concentration of PhSeSePh. The reaction with PhSeSePh is similar to the reaction with PhSSPh with respect to the spectral signature of the resulting **1**-[η^1-NC(EPh)NMe$_2$] species.

At −40 °C, the reaction proceeds with PhEEPh (E = S, Se) as seen at lower temperatures; however, the rates of the formation of **1**-[η^1-NC(EPh)NMe$_2$] and the conversion from **1**-[η^1-NCNMe$_2$] to **1**-[η^2-NCNMe$_2$] are more competitive. Although the PhEEPh can trap the **1**-[η^1-NCNMe$_2$] complex, the conversion rate to the **1**-[η^2-NCNMe$_2$] complex is more rapid. To make trapping by PhEEPh more competitive its concentration can be increased. This change can be qualitatively observed as the λ of the low energy transition shifts from the dominant **1**-[η^1-NC(SPh)NMe$_2$] species at λ = 636 nm to the increasing appearance of the **1**-[η^2-NCNMe$_2$] species at λ = 650 nm (Figure S18).

Finally, it was of interest to compare the reactivity of the two in situ generated radicals **1**-[η^1-NCPh] and **1**-[η^1-NCNMe$_2$] toward oxidative addition by PhSSPh at low temperature. As shown in Figure S19, under comparable conditions in which **1**-[η^1-NCNMe$_2$] was found to react, no reaction of **1**-[η^1-NCPh] and PhSSPh was observed (as predicted from the activation parameters for this reaction described above) confirming the much faster rate of oxidative addition of in situ generated **1**-[η^1-NCNMe$_2$] relative to **1**-[η^1-NCPh].

Computational Analysis of Binding of PhCN and Me$_2$NCN as both η^1 and η^2 Ligands to 1 in Both Doublet and Quartet States. Density functional theory (DFT) calculations of the **1**-[NCNMe$_2$] and **1**-[NCPh] adducts both as η^1 and η^2 species in both doublet and quartet states were carried out in the current study to gather knowledge about the structure and preferred hapticity in these complexes and to further confirm the nature of the observed intermediate in the stopped-flow experiments as **1**-[η^1-NCNMe$_2$]. Binding of nitriles in the quartet state was found to be repulsive for all the species and leads to dissociation of the ligand. Correspondingly, no minima were found in the quartet state for any of the complexes explored. A summary of selected bonds and angles calculated at the BP86/6-311G(d,p) (MWB28 with an additional set of f functions for Mo) level of the **1**-[NCNMe$_2$] and **1**-[NCPh] adducts in the doublet state is collected in Table S2. For **1**-[η^2-NCNMe$_2$], the only compound calculated for which the X-ray structure has been previously determined, computed and experimental geometries are in good agreement. The main difference between the computed structures of **1**-[η^1-NCPh] and **1**-[η^1-NCNMe$_2$] is the angle N−C−R. Whereas the N−C−R moiety in **1**-[η^1-NCPh] is essentially linear, the same arrangement in **1**-[η^1-NCNMe$_2$] forms an angle of 127.7°. In addition the Mo−N bonds are shorter in the Me$_2$NCN adducts. Since the Me$_2$NCN ligand is smaller, it can approach closer to the Mo and maximize the bonding interaction; however, steric hindrance prohibits a closer approach of the bulkier PhCN ligand. The amide N exhibits trigonal planar geometry in **1**-[NCNMe$_2$] for both η^1 and η^2 conformers. This behavior has been previously reported for other complexes such as *trans*-[Mo(N$_2$)(NCNEt$_2$)(dppe)$_2$],[15] W(P[^{i}Pr]$_3$)$_2$(CO)$_3$(Me$_2$NCN),[16] Cr(CO)$_5$(NCNEt$_2$),[37] and *trans*-[Fe(Et$_2$PCH$_2$CH$_2$PEt$_2$)$_2$(NCNEt$_2$)$_2$][BF$_4$]$_2$.[38]

DFT calculations at the BP86/6-311G(d,p) (MWB28 with an additional set of f functions for Mo) level predict a ΔE_0 = −16.3 kcal mol^{-1} for formation of **1**-[η^1-NCPh] which compares to the experimentally determined value of ΔH = −14.5 ± 1.5 kcal mol^{-1}. For the formation of **1**-[η^2-NCPh], ΔE_0 = −10.3 kcal mol^{-1}, implying that for PhCN the η^2 binding motif is less stable than is the η^1. For generation of **1**-[η^1-NCNMe$_2$], ΔE_0 = −20.1 kcal mol^{-1} and for **1**-[η^2-NCNMe$_2$], ΔE_0 = −23.2 kcal mol^{-1} for the formation of the η^2-adduct. The computed energy for **1**-[η^1-NCPh] and **1**-[η^2-NCNMe$_2$] is in good agreement with the experimentally determined values. Calculations predict a more stable η^1 conformation for the PhCN adduct by 6 and 7.5 kcal mol^{-1} at the BP86 and B3LYP levels, respectively. However, for the Me$_2$NCN complex, the η^2 was found to be 3.1 (BP86) and 2.3 (B3LYP) kcal mol^{-1} more stable than the η^1 isomer. The entropies were calculated to be −48, −57, −58, and −61 cal mol^{-1} K^{-1} at the BP86/LANL2Z level for formation of **1**-[η^1-NCPh], **1**-[η^2-NCPh], **1**-[η^1-NCNMe$_2$], and **1**-[η^2-NCNMe$_2$], respectively, from the metallic and ligand fragments.

Table 4. Computational Vibrational Data for Binding of Nitriles to **1**. All Values in cm^{-1}

calcuation level	$\nu_{C\equiv N}$ free	$\nu_{C\equiv N\eta1}$ bound	$\Delta\nu_{C\equiv N(\eta1)}$	$\nu_{C\equiv N\eta2}$ bound	$\Delta\nu_{C\equiv N(\eta2)}$
		PhCN			
BP86/LANL2Z	2169	2009	160	1580	589
B3LYP/LANL2Z	2262	2118	144	1678	584
		Me$_2$NCN			
BP86/LANL2Z	2168	1618[a]	550	1585	583
B3LYP/LANL2Z	2249	1700[a]	549	1640	609

[a] The intensity of the band was computed to be 10 times weaker than that for the corresponding PhCN derivative.

Table 4 collects the computational vibrational data for binding of nitriles to **1** at the BP86/LANL2Z and B3LYP/LANL2Z levels. The calculated IR frequencies are in good agreement to those obtained experimentally (see Table 1).

The electronic transitions of **1**-[η^1-NCNMe$_2$] and **1**-[η^2-NCNMe$_2$] were computed by time-dependent density functional

(37) Ohnet, M.-N.; Spasojevic-de Brie, A.; Dao, N. Q.; Schweiss, P.; Braden, M.; Fischer, H.; Reindl, D. *J. Chem. Soc., Dalton Trans.* **1995**, 665.

(38) Martins, L. M. R. D. S.; Fraústo da Silva, J. J. R.; Pombeiro, A. J. L.; Henderson, R. A.; Evans, D. J.; Benetollo, F.; Bombieri, G.; Michelin, R. A. *Inorg. Chim. Acta* **1999**, *291*, 39.

Table 5. Mulliken Spin Densities Calculated at the BP86/6-311G(d,p) (MWB28 with an Additional Set of f Functions for Mo) Level

atom	**1**-[η^1-NCPh]	**1**-[η^2-NCPh]	**1**-[η^1-NCNMe$_2$]	**1**-[η^2-NCNMe$_2$]
Mo	+0.81	+0.86	+0.83	+0.81
$N_{nitrile}$	−0.08	+0.08	−0.04	+0.10
$C_{nitrile}$	+0.23	−0.06	+0.08	−0.05
N(Me$_2$)			+0.09	−0.01
$N_{anilides}$	−0.02, −0.03, +0.06	+0.04, +0.04, −0.3	−0.03, <0.01, <0.01	+0.06, +0.03, −0.01

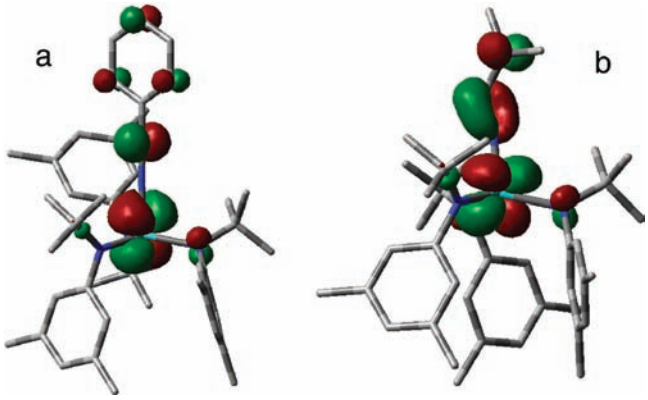

Figure 10. SOMOs of **1**-[η^1-NCPh] (a) and **1**-[η^1-NCNMe$_2$] (b) calculated at the BP86/6-311G(d,p) (MWB28 with an additional set of f functions for Mo) level.

theory (TD-DFT) calculations at the BP86/6-311G(d,p) (MWB28 with an additional set of f functions for Mo) level. The computed transitions are red-shifted by ~50 nm as values of $\lambda = 507$ nm ($f = 0.0190$) and 706 nm ($f = 0.0060$) were obtained for the η^1 and η^2 isomers, respectively. Whereas, the experimentally determined values, by UV−vis spectroscopy, are $\lambda = 456$ nm ($\varepsilon = 5670$ M^{-1} cm^{-1}) and $\lambda = 650$ nm ($\varepsilon = 1000$ M^{-1} cm^{-1}) for the η^1 and η^2 adducts. The agreement between the computed and experimentally determined electronic transitions is reasonably good.

Mulliken spin densities calculated at the same level of theory are collected in Table 5 and show that the spin densities are mainly located in the metal for all complexes. For **1**-[η^1-NCPh] a large contribution in the nitrile C (+0.23) was obtained. This spin localization in the carbon accounts for the observed C radical character and therefore the reactivity observed for the complex.[23−27] In addition, there is not a large delocalization of the spin density in the ring in **1**-[η^1-NCPh] (<0.01 for all the C but −0.03 (C_{ipso}) and +0.01 (C_{ortho})). Furthermore, the Mulliken spin densities calculated for C and N in C≡N have opposite signs in the η^1 and η^2 adducts.

The calculated singly occupied molecular orbitals (SOMOs) for the η^1 complexes shown in Figure 10 clearly contrast the essentially linear nature of **1**-[η^1-NCPh] (which retains sp hybridization at C) with the angular nature of **1**-[η^1-NCNMe$_2$] (which converts to sp^2 hybridization at C). It should be noted that the drawings in Figure 10 reflect the spatial extension of orbital contours and not the net Mulliken spin density.

In Figure 10 the d-orbitals do not appear large due to their relatively compact nature. In spite of that, the majority of the spin density (>80%) resides in a relatively inaccessible Mo based d orbital for both η^1 complexes. For **1**-[η^1-NCPh] the 23% spin density located on the C atom appears in a relatively compact 2p orbital and small residual contributions can be seen in the arene ring and coordinated amides. For **1**-[η^1-NCNMe$_2$], the

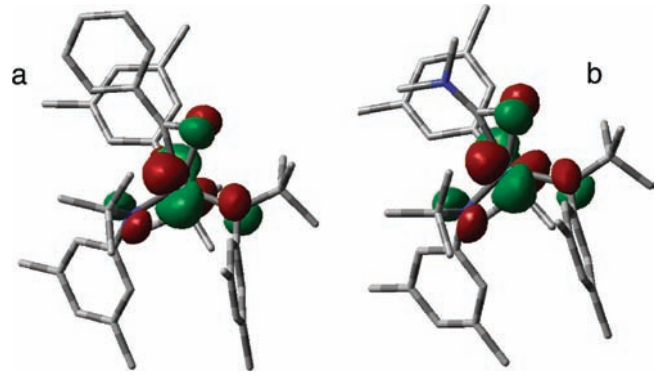

Figure 11. SOMOs of **1**-[η^2-NCPh] (a) and **1**-[η^2-NCNMe$_2$] (b) calculated at the BP86/6-311G(d,p) (MWB28 with an additional set of f functions for Mo) level.

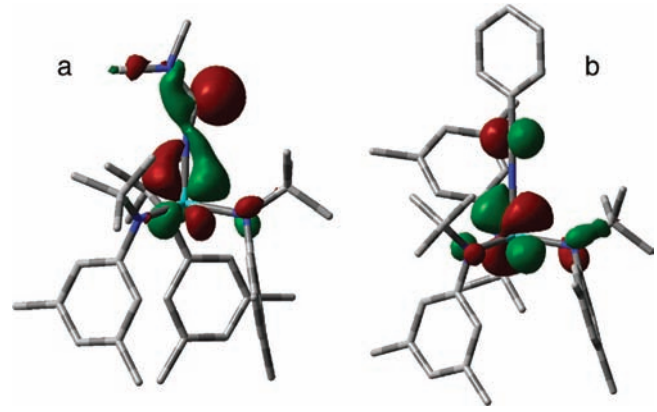

Figure 12. HOMOs of **1**-[η^1-NCNMe$_2$] (a) and **1**-[η^1-NCPh] (b) calculated at the BP86/6-311G(d,p) (MWB28 with an additional set of f functions for Mo) level.

8% spin density on the C atom, and 9% spin density on the N atom of the NMe$_2$ group are more diffuse. Though the data in Table 5 show that **1**-[η^1-NCNMe$_2$] has a smaller Mulliken spin density on C compared to **1**-[η^1-NCPh], the SOMO picture in Figure 10 shows that for **1**-[η^1-NCNMe$_2$] this reduced spin density is in a more diffuse and sterically accessible orbital.

The calculated SOMOs for the η^2 complexes shown in Figure 11 display similar shapes and electron distributions for both **1**-[η^2-NCPh] and **1**-[η^2-NCNMe$_2$]. Aside from the large electron density concentrated in a Mo d orbital, there is a significant Mulliken spin density on the N atom; this appears to be in a sterically more protected area. Most notable is the absence of spin density on the C atom which is the reacting atom.

Finally, the computed contour diagrams for the HOMO orbitals of both η^1 complexes are shown in Figure 12. While these are complex delocalized molecular orbitals, the lone pair character of the rehybridized C atom of **1**-[η^1-NCNMe$_2$] from sp to sp^2 is evident. This accounts for the differences in computed vibrational spectra of the two complexes and severe reduction to lower wavenumbers for **1**-[η^1-NCNMe$_2$].

Discussion

The goal of this work was to determine the thermodynamic and kinetic parameters distinguishing η^1 and η^2 binding of nitriles to **1** and to characterize the radical-like reactivity of both η^1 and η^2 nitrile complexes. Despite considerable previous study[23−27] of the reactivity of **1**-[η^1-NCPh] and report of the structure of **1**-[η^2-NCNMe$_2$][23] fundamental aspects of their

Table 6. Selected Activation Parameters and Thermodynamic Data for Nitrile Binding

	1-[η^1-NCPh]	**1**-[η^1-NCMes]	**1**-[η^1-NCAd]	**1**-[η^1-NCNMe$_2$]	**1**-[η^1-CNAd][a]
$\Delta H^{\ddagger}_{on}$	5.2 ± 0.2	5.0 ± 0.3	5 ± 1	6.4 ± 0.4	5.5 ± 0.5
$\Delta S^{\ddagger}_{on}$	−24 ± 1	−26 ± 1	−28 ± 5	−18 ± 2	−15
ΔH^{o}	−14.5 ± 1.5	−15.4 ± 1.5	−6 ± 2	−17 ± 3[b]	−29.4 ± 0.4
ΔS^{o}	−40 ± 5	−52 ± 5	−20 ± 7		

[a] Data taken from ref 28. [b] This value is an estimate based on computational data and experimental observations, see text for discussion.

binding to form these two disparate bound radicals have not been reported to date. In addition, one electron oxidation by PhSSPh presents the opportunity to compare reaction mechanisms for what in valence bond formalism might be viewed as a Mo(IV)-bound nitrile radical complex in **1**-[η^1-NCPh] and a Mo(V) metallocycle radical complex in **1**-[η^2-NCNMe$_2$]. Kinetic, thermodynamic, and computational data for nitrile binding and activation in initial η^1 hapticity, reversible isomerization to η^2 hapticity, and oxidative addition by PhSSPh, according to the general mechanism shown in Scheme 1, have been determined and are discussed in separate sections below.

Formation and Properties of 1-[η^1-NCR] Complexes. The paramagnetic ($S = {}^3/_2$) complex **1** presents an unusual and selective ligand binding pattern. Coordination of ligands to **1** generally involves pairing of the electrons on the metal, at least partial electron transfer to the ligand, and geometrical rearrangements at the sterically demanding Mo(III) metal center. As discussed ealier, there is a large shift to lower wavenumber upon coordination of the coordinated nitrile stretching frequency. Typical shifts of η^1-coordinated nitriles are illustrated by the work of Taube and co-workers[39] who reported a shift to higher wavenumber ($\Delta\nu = +39$ cm^{-1}) for Ru(NH$_3$)$_5$(NCPh)$^{3+}$ but to lower wavenumber ($\Delta\nu = -44$ cm^{-1}) for Ru(NH$_3$)$_5$(NCPh)$^{2+}$. The observed shifts in nitrile stretching frequency for **1**-[η^1-NCR] are in the same region as gas phase time-resolved (TR)-IR spectroscopy assignments of $\nu_{C\equiv N}$ for photogenerated nitrile radical anions[40] and suggest significant electron transfer and radical character associated with the bound nitrile ligand. The arene nitriles, PhCN and MesCN, show more significant shifts to lower energy than does AdCN; however, its shift is also significant and implies occupation of the antibonding π^* orbitals of the nitrile.

Since catalytic reactions generally cannot occur faster than rates of ligand binding and exchange, data in this area are always essential to understanding chemical transformations. Combined activation parameters and thermodynamic data for nitrile binding are collected in Table 6.

The enthalpies of activation show surprisingly little variation. Differences in rate constants appear to be controlled primarily by entropies of activation which show larger variation than do corresponding enthalpies of activation. Qualitatively this may mean that the transition state for binding of AdNC for example, the strongest ligand in this set, requires a less restrictive arrangement of the ligand set on **1**. Despite the fact that these reactions are rapid and the enthalpy of activation is low, 5.5 ± 0.5 kcal mol^{-1}, it is not as low as those which can occur when a donor ligand approaches a truly vacant site in a metal complex.[41] Contributions to the enthalpy of activation may be due to steric rearrangements at the crowded metal center, or to electronic rearrangements including spin pairing. A notable exception to this ligand binding profile is •NO which binds at a rate too fast to measure using conventional methods.[42]

Thermodynamic data in Table 6 span a much greater range of binding enthalpies than are typically seen for nitrile binding to low valent spin paired complexes such as Mo(CO)$_3$(P[^{i}Pr]$_3$)$_2$ (see eq 1). While there is no doubt that steric factors play a dominant role in ligand binding to **1**, electronic factors may be even more important. For the complexes **1**-[η^1-NCAd] and **1**-[η^1-CNAd] the steric ligand profile must be similar, yet the difference in enthalpies of binding, ≈ 24 kcal mol^{-1} is a much larger difference than typically seen in comparative thermochemistry of nitriles and isonitriles in binding to transition metals.[16,28,43]

Computational studies played a key role in formulation of the intermediate complex with $\lambda = 456$ nm detected in stopped flow studies as being **1**-[η^1-NCNMe$_2$]. On the basis of the absence of a nitrile band in the IR in the expected region 1800−2300 cm^{-1} in spectroscopic studies done at −80 °C, it was considered possible that this intermediate might be either a high-spin adduct or a conformational isomer of the η^2 complex. However, computations indicated that none of the nitrile complexes were stable in high spin ($S = {}^3/_2$) states and effectively ruled out that possibility. The computed structure of **1**-[η^1-NCNMe$_2$] was found to differ significantly from that of **1**-[η^1-NCPh] in that for the "push-pull" nitrile Me$_2$NCN, involvement of the lone pair of electrons on the dimethyl amine group cause rehybridization of the C atom to sp^2 hybrid and an even more drastic reduction in the bond order and stretching frequency of the nitrile due to this effect abetted by donation of electron density from **1**. The computed UV−vis spectral data support this as do computed vibrational data which are shifted close to 1600 cm^{-1} to essentially a C═N area. The computed thermodynamic bond strength of **1**-[η^1-NCNMe$_2$] place it as being more strongly held than PhCN. This surprising prediction was shown to hold true in kinetic studies where the rate of dissociation of Me$_2$NCN from **1**-[η^1-NCNMe$_2$] showed a smaller value for k_{-1} than that found for **1**-[η^1-NCPh]. The generally good agreement between calculated and observed spectroscopic and thermodynamic data for other complexes accessible to more extensive experimental probing give confidence to assignment of the structure and properties of the initial product of interaction as being **1**-[η^1-NCNMe$_2$].

Formation and Properties of the 1-[η^2-NCR] Complexes. Thermodynamic studies showed that the enthalpy of formation of **1**-[η^2-NCNMe$_2$] was approximately 7 kcal mol^{-1} more exothermic than **1**-[η^1-NCPh]. Conventional kinetic studies showed that ligand substitution reactions of **1**-[η^2-NCNMe$_2$] by AdNC had an enthalpy of activation of ∼25 kcal mol^{-1} and occurred by a fully dissociative pathway, presumably through formation first of **1**-[η^1-NCNMe$_2$] followed by dissociation of Me$_2$NCN in this high activation enthalpy process. The enthalpy

(39) Sekine, M.; Harman, W. D.; Taube, H. *Inorg. Chem.* **1988**, *27*, 3604.
(40) $\nu_{C\equiv N}$ for the Me$_2$NC$_6$H$_4$CN radical anion were located at 2096 cm^{-1} for the singlet state and 2040 cm^{-1} for the triplet state: Hashimoto, M.; Hamaguchi, H *J. Phys. Chem.* **1995**, *99*, 7875.
(41) Yang, H.; Kotz, K. T.; Asplund, M. C.; Wilkens, M. J.; Harris, C. B. *Acc. Chem. Res.* **1999**, *32*, 551.
(42) The reason for the significantly faster rate of binding of this small, paramagnetic ligand is not resolved. For rate data on binding of NO see: Cherry, J. P. F.; Johnson, A. R.; Baraldo, L. M.; Tsai, Y. -C.; Cummins, C. C.; Kryatov, S. V.; Rybak-Akimova, E. V.; Capps, K. B.; Hoff, C. D.; Haar, C. M.; Nolan, S. P. *J. Am. Chem. Soc.* **2001**, *123*, 7271.
(43) These data imply that the isomerization reaction AdCN-**1** → AdNC-**1** should be thermodynamically favorable by ∼10 kcal mol^{-1}, compared to the same reaction for AdCN-Mo(CO)$_3$(P[*i*-Pr]$_3$)$_2$ which is approximately thermoneutral,[16] and the recently computed endothermic enthalpies of this isomerization reported for main group compounds: Timoshkin, A. Y.; Schaefer, H. F. *J. Am. Chem. Soc.* **2003**, *125*, 9998.

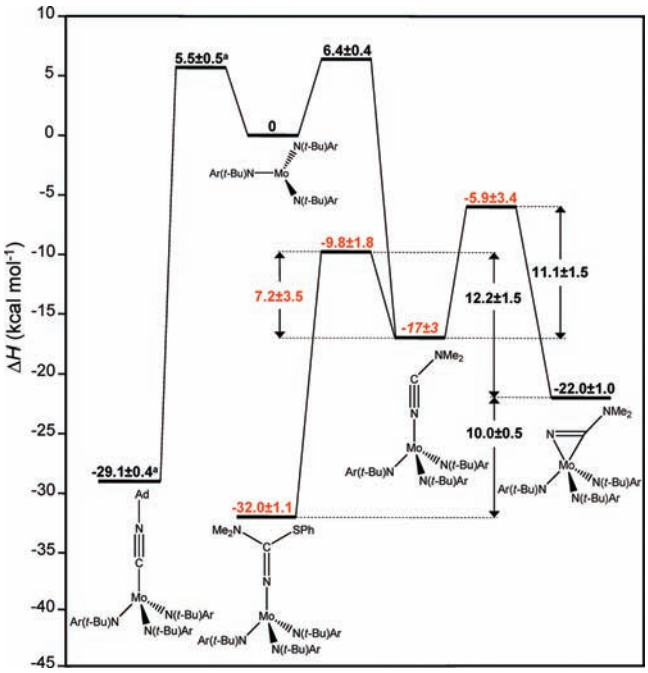

Figure 13. Combined potential energy diagram; enthalpies of reaction and activation in kcal mol^{-1}. [a] Taken from ref 28.

of oxidative addition for PhSSPh reacting with **1**-[η^2-NCNMe$_2$] was lower than that ($\sim$10 kcal mol^{-1}) and is presumed to occur by reversible formation of **1**-[η^1-NCNMe$_2$] which then reacts with PhSSPh.

Computational studies show remarkably similar structures for **1**-[η^2-NCR] for R = Ph and NMe$_2$. Presumably for steric reasons, the η^2 isomer is computed to be $\sim$6 kcal mol^{-1} *less* stable than the η^2 binding hapticity in the case R = Ph. For the smaller Me$_2$NCN ligand the situation is reversed and the η^2 isomer is computed to be $\sim$3 kcal mol^{-1} *more* stable. The fact that this is probably a steric factor is supported by the observation that for the complex between PhCN and "Mo(N[^{i}Pr]Ar)$_3$"[44] the η^2 binding hapticity is experimentally observed to be the most stable structural isomer.

Stopped flow kinetic studies allowed accurate assessment of the rate of the isomerization reaction converting **1**-[η^1-NCNMe$_2$] to **1**-[η^2-NCNMe$_2$]. Derived activation parameters for this process are: $\Delta H^{\ddagger}_{k2} = 11.1 \pm 0.2$ kcal mol^{-1}, $\Delta S^{\ddagger}_{k2} = -7.5 \pm 0.8$ cal mol^{-1} K^{-1}. The enthalpy of activation is a significant fraction of the bond energy itself (assigned as 17 ± 3 kcal mol^{-1}) but does not have an extremely unfavorable entropy of activation. Further study of the reaction mechanism for this change in hapticity by computational methods is planned.[45]

Oxidative Addition of PhSSPh and Low-Temperature Trapping of in Situ Generated 1-[η^1-NCNMe$_2$]. The most surprising aspect of this work, that reaction of **1** with a mixture of Me$_2$NCN/PhSSPh will occur faster at -80 °C than at room temperature, is fully consistent with the potential energy diagram shown in Figure 13. The oxidative addition reaction between **1**-[η^1-NCNMe$_2$] and PhSSPh occurs relatively rapidly at -80 °C because **1**-[η^1-NCNMe$_2$] can be trapped prior to its isomerization to **1**-[η^2-NCNMe$_2$] at low but not at high temperature. The fact that isomerization, the k_2 step in eq 7, has an enthalpy of activation of 11 kcal mol^{-1} compared to the estimated 6 kcal mol^{-1} enthalpy of activation for oxidative addition of PhSSPh (which has a more unfavorable entropy of activation) has the practical consequence that at high temperatures the rate of isomerization will eclipse that of oxidative addition. Thus if **1**-[η^1-NCNMe$_2$] is successfully trapped in its first pass through, oxidative addition will be successful. However if this opportunity is missed and **1**-[η^1-NCNMe$_2$] is allowed to isomerize to **1**-[η^2-NCNMe$_2$] then severe retardation of the oxidative addition step will occur.

Comparing Reactivity of 1-[η^1-NCR] and 1-[η^2-NCR] Complexes: Combined Reaction Profile. For the dimethyl cyanamide system a combined potential energy diagram (enthalpy of reaction) for all reactions studied here is assembled in Figure 13 which is consistent with all experimental kinetic and computational data. It is postulated that reactions of **1**-[η^2-NCNMe$_2$] proceed through initial formation of metastable **1**-[η^1-NCNMe$_2$].

A key point in Figure 13 is "anchoring" of the data for the enthalpy of binding of Me$_2$NCN to **1** to form **1**-[η^1-NCNMe$_2$]. The assigned enthalpy of **1**-[η^1-NCNMe$_2$] at $\Delta H = -17 \pm 3$ kcal mol^{-1} overlaps with kinetic and computational estimates of this bond strength.[46] All other data are derived from experimental enthalpies of reaction and activation enthalpies. The potential well stabilizing **1**-[η^1-NCNMe$_2$], activation parameters for isomerization of **1**-[η^1-NCNMe$_2$] to **1**-[η^2-NCNMe$_2$], as well as binding and dissociation and oxidative addition reactions are all derived and serve to present a reasonably complete view of reactivity in this system. A summary of key steps is presented below:

(i) Binding of Me$_2$NCN, which involves a spin state change from $S = {}^3/_2$ to $S = {}^1/_2$ and electron transfer from the metal to the ligand occurs with an enthalpy of activation of 6.4 kcal mol^{-1} and is rapid even at low temperature.

(ii) Once formed, **1**-[η^1-NCNMe$_2$] can convert to **1**-[η^2-NCNMe$_2$] which is a first order reaction with a (relatively) high enthalpy of activation of 11.1 kcal mol^{-1}. At low temperatures this reaction is slow enough to allow trapping, but at higher temperatures it gains in rate more rapidly than other processes with lower enthalpies of activation. As a result the ability to detect and/or trap **1**-[η^1-NCNMe$_2$] is gone at high temperatures.

(iii) The rate of oxidative addition of PhSSPh to **1**-[η^1-NCNMe$_2$] (formed either in a low temperature trapping experiment or a high temperature isomerization) is fast. It is faster than the comparable reaction of **1**-[η^1-NCPh] in spite of the latter complex having a higher spin density on the reactive C atom. This is presumably due to the geometric change on rehybridization which occurs for the "push−pull" nitrile.

(44) "Mo(N[*i*-Pr]Ar)$_3$" is the isopropyl derivative which is actually a Mo(V) hydride complex in which one C-H bond of an isopropyl group has undergone oxidative addition at Mo. This complex serves as a "masked" form of the Mo(III) complex, see: Tsai, Y.-C.; Johnson, M. J. A.; Mindiola, D. J.; Cummins, C. C.; Klooster, W. T.; Koetzle, T. F. *J. Am. Chem. Soc.* **1999**, *121*, 10426.

(45) Germain, M. E.; Temprado, M. Rybak-Akimova, E. V.; Cummins, C. C.; Hoff, C. D, unpublished results.

(46) The kinetic estimates are qualitative and based on the observed input of k_{-1} for dissociation of **1**-[η^1-NCNMe$_2$] becoming significant in a temperature range comparable to but somewhat higher than that of PhCN. Assuming comparable entropies of binding, the enthalpy of binding of **1**-[η^1-NCNMe$_2$] would thus be expected to be somewhat more favorable than -14.5 ± 1.5 kcal mol^{-1}. It is clearly less favorable than the **1**-[η^2-NCNMe$_2$] complex at -22 kcal mol^{-1}. Computational estimates place **1**-[η^1-NCNMe$_2$] approximately 3 kcal mol^{-1} above **1**-[η^2-NCNMe$_2$] and hence would predict an enthalpy of binding of **1**-[η^1-NCNMe$_2$] of -19 kcal mol^{-1}. The assigned value of -17 ± 3 kcal mol^{-1} overlaps within experimental error both kinetic and computational estimates.

Conclusions

This paper provides fundamental rate and energetic data for binding of nitriles to a paramagnetic complex and reactivity of the resulting "bound radical complex". Nitrile binding to $Mo(N[^tBu]Ar)_3$ does not correspond to simple association of the lone pair of electrons with a vacant orbital on the metal complex. The $S = {}^3/_2$ complex does not have a readily available low energy orbital for binding and formation of an "inner sphere" complex necessarily involves spin pairing at the metal to form a vacant orbital. It also incorporates at least partial electron transfer from the metal to nitrile to form what could be viewed as a bound radical nitrile anion complex $[R\text{-}C(\bullet)N]^{\delta-}[Mo(N[^tBu]Ar)_3]^{\delta+}$. Strong evidence for electron transfer in these systems is found in the large shifts of the nitrile stretch to lower frequency upon coordination ($150-400\ cm^{-1}$).

The large difference in the enthalpies of binding of AdCN (-6 kcal/mol^{-1}) and PhCN (-14.5 kcal mol^{-1}) may be due to steric and electronic factors related to more favorable charge delocalization for the aromatic nitrile, PhCN. Surprisingly, computations conclude that binding of Me_2NCN to **1** would be even stronger than binding of PhCN in a η^1 mode. This is attributed to active participation of the lone pair of electrons on the Me_2N group in the complex **1**-[η^1-$NCNMe_2$] and concomitant rehybridization of the C atom of the nitrile.

The rates and associated activation parameters were found to be quite similar for the different nitriles studied in terms of rates of ligand binding ($k_1 = k_{on}$). Differences in K_{eq} (k_1/k_{-1}) values for binding are due primarily to the large differences found in rates of nitrile dissociation ($k_{-1} = k_{off}$). The rate of conversion of the η^1 and η^2 complexes between **1** and Me_2NCN is slow enough that at low temperatures it may be detected and also used as an in situ reagent which is orders of magnitude more reactive than its η^2 isomer.

Binding in an η^2 mode is generally viewed as resulting in "greater activation" of a ligand compared to η^1 hapticity. In agreement with that, computational structural data indicate that the C−N bond of the coordinated nitrile does in fact undergo more bond lengthening in the η^2 mode of binding than for η^1 for both benzonitrile and dimethyl cyanamide. In terms of one electron oxidation by PhSSPh, however, it is the η^1 complex that is most reactive. *The complex with the more lengthened C−N bond will be more reactive only if it is closer to the transition state for the desired reaction.* In the one electron oxidation reaction studied here, the **1**-[η^1-$NCNMe_2$] was found to be sufficiently reactive that, provided it could be intercepted before forming the more stable η^2 derivative, oxidative addition occurred within seconds at -80 °C. If allowed to isomerize to the more thermodynamically stable η^2 isomer, reactivity effectively ceases.

Differences in reactivity cannot be assigned in a simple way to differences in the amount of spin density on the reactive C atom of the bound nitrile. Computational results showed that for the highly delocalized SOMOs the majority of the spin density (>80%) remains located on the metal center for all the complexes. Distribution of the remaining ∼20% spin density to the other atoms depended strongly on the specific nitrile and its hapticity. Despite having a lower spin density on the reactive C atom, **1**-[η^1-$NCNMe_2$] (8%) was found to react faster with PhSSPh than **1**-[η^1-NCPh] (23%). The observed faster rate of oxidation of **1**-[η^1-$NCNMe_2$] compared to **1**-[η^1-NCPh] (despite a lower spin density on the C atom) is ascribed to the rehybridized nature of central carbon of the "push−pull" nitrile bringing it closer to the transition state.

Successful detection, characterization, and interception of **1**-[η^1-$NCNMe_2$] has been achieved on a quantitative basis as shown in Figure 13 which summarizes our best view of reactivity in this system. The ability to intercept the η^1 complex prior to its isomerization was predicted in advance of observation and provides hope that catalyst design by reaction engineering may be achieved once a manifold of reactions are well understood on a quantitative basis. A target of more interest would be the adduct formed between dinitrogen and **1** ($[(\bullet)NN]^{\delta-}[Mo(N[^tBu]Ar)_3]^{\delta+}$) which is a presumed intermediate on the reaction coordinate leading to $[\mu\text{-}N_2][Mo(N[^tBu]Ar)_3]_2$. The large differences in reactivity observed for the simple nitrile complexes studied here suggest that direct extrapolation of results to N_2 is not justified, although general principles of radical couplings might be applicable to dinitrogen activation by transition metal complexes. For reactive paramagnetic complexes no simple picture has emerged as yet. On the basis of the large differences in reactivity of the bound nitrile radical complexes studied, the extent to which results for nitriles can be compared to dinitrogen presents a challenge. The work reported here provides a solid basis for such comparison, and experimental and computational investigation of dinitrogen and other N donor ligands binding to $Mo(N[^tBu]Ar)_3$ is in progress.

Acknowledgment. Support of this work by the National Science Foundation (Grant No. CHE 0615743, (CDH) CHE 0750140 (ERA); CHE 0719157 (CCC) is gratefully acknowledged. M.T. thanks the Spanish Ministry of Science and Innovation and the Fulbright commission under Fellowship FU-2006-1738. The rapid kinetics instrumentation at Tufts was supported by the NSF (CRIF program, Grant CHE 0639138). The authors also thank Prof. Obis D. Castaño (Universidad de Alcalá de Henares) for help in computational chemistry and Jared Silvia (MIT) for help in structural data analysis.

Supporting Information Available: Information on preparation of complexes and standard techniques used in physical measurements; experimental procedure description, spectroscopic, kinetic, thermodynamic and computational Figures and Tables, and CIF file for crystal structure determination of **1**-[η^1-$NC(SPh)NMe_2$]. This material is available free of charge via the Internet at http://pubs.acs.org.

JA905849A